Scanning Microscopy

9-30-1996

Secondary Electron Emission from Simple Metals: Comparative Studies for Al, Mg, and Be

M. Rosler
Humboldt-University Berlin, max.roesler@gmx.de

Recommended Citation

Utah State University
MERRILL-CAZIER LIBRARY

SECONDARY ELECTRON EMISSION FROM SIMPLE METALS: COMPARATIVE STUDIES FOR Al, Mg, AND Be

M. Rösler[*]

Department of Physics, Humboldt-University Berlin
Invalidenstr. 110, 10115 Berlin, Germany

Abstract

In the secondary electron emission (SEE) from solids, the role of different excitation processes is now as ever of special interest from both the theoretical and the experimental points of view. Depending on the primary energy, the relative importance of different excitation mechanisms related to conduction as well as core electrons will be discussed for different simple metals. So far, first principles results are available only for Al for primary energies up to 10 keV. Starting from a microscopic description of the SEE based on the transport equation formalism, calculations were performed for other nearly-free-electron metals (Mg, Be) up to primary energies used in scanning electron microscopy. In this way, it is possible to obtain more general statements about the role of different excitation processes responsible for SEE. Special attention is devoted to the contribution of emitted electrons stemming from the excitation of conduction electrons by decay of bulk plasmons generated by the primary electron. The different strength of this excitation mechanism in Al, Mg, and Be is related to the different magnitude of the plasmon damping in these metals.

Key Words: Secondary electron emission, electron yield, Boltzmann equation, excitation process, transport process, escape process, plasmon creation, plasmon decay, core ionization, auger process, mean free path, energy distribution, angular distribution.

[*]Address for correspondence:
Max Rösler
Karl-Pokern-Str. 12
D-12587 Berlin, Germany
                Telephone number: (030) 645-7154
                     FAX number: (030) 645-1950
                     E-mail: max.roesler@gmx.de

Introduction

Secondary electron emission (SEE) is one of the most interesting consequences of the inelastic interaction between the incident primary electrons (PE) and the solid state electrons. Different processes of secondary electron (SE) generation are responsible for the emission phenomenon. The relative importance of these excitation mechanisms depends, among other things, on the energy of the impinging PE. Up to now, calculations of the emission characteristics only exist for the nearly-free-electron (NFE) metal Al (Rösler and Brauer, 1991). Starting from a transport equation formalism, first principles expressions for the excitation and scattering rates were used in these calculations. Besides our own work (Rösler and Brauer, 1981a,b, 1988, 1991), there are other authors who prefer the transport equation formalism using a microscopic description of different scattering quantities (Bindi et al., 1980a,b, 1987, 1988; Devooght et al., 1987, 1991, 1992; Dubus et al., 1987, 1990), or a description based on similar principles to sputtering theory (Schou, 1980, 1988). For a number of materials, including Al, calculations were performed within Monte-Carlo schemes using simplified expressions for the different basic scattering quantities (Koshikawa and Shimizu, 1974; Shimizu et al., 1976; Ganachaud and Cailler, 1979a,b; Ding and Shimizu, 1988; Cailler and Ganachaud, 1990a,b; Kotera et al., 1990; Luo and Joy, 1990; Devooght et al., 1991; Akkerman et al., 1992, 1993; Shimizu and Ding, 1992; Dubus et al., 1993; Kawata and Ohya, 1994; Ohya, 1994). Especially, the ionization of core levels by the impinging PE as well as by excited electrons will be described using Gryzinski's formula (Gryzinski, 1965a,b,c).

One of the most important applications of SEE is scanning electron microscopy. In this case, the SE signal is the indicator of the surface topography. The problems which are related to this application of SEE are comprehensively reviewed by Seiler (Seiler, 1983, 1984). It was shown (Ritchie, 1981; Ritchie et al., 1990, 1991) from a theoretical point of view that in the scanning transmission electron microscope (STEM), it is

Table of Symbols

SEE	Secondary electron emission	l^{inel}	Inelastic mean free path of the electron
PE	Primary electron		
SE	Secondary electron	P_l	Legendre polynomial of lth order
NFE	Nearly-free electron	N_l, S_l, W_l^σ	Expansion coefficients of density, excitation function, and transition function with respect to Legendre polynomials
STEM	Scanning transmission electron microscope		
E	Electron energy		
$\vec{u}$	Momentum direction of the electron	$W^{(el)}$	Contribution of elastic scattering processes to the total transition function
$j(E,\vec{u})$	Energy and angle dependent current density		
E_0	Primary energy	$W^{\sigma(inel)}$	Contribution of inelastic scattering processes to the total transition function
$j(E)$	Energy distribution of emerging electrons		
σ	Total electron yield	PWEM	Partial wave expansion method
δ	Yield of true secondary electrons	RPA	Random phase approximation
η	Yield contribution of backscattered electrons	$\hbar$	Reduced Planck constant
		ω_p	Plasma frequency
δ_0	Contribution of the incident electron to the true secondary yield	S_p	Excitation function related to plasmon decay
$j_i(E',\vec{u}')$	Current density of inner excited electrons	S_e	Excitation function related to direct excitation of conduction electrons
$N(E',\vec{u}')$	Density of inner excited electrons	S_c	Excitation function related to direct excitation of core electrons
$N(x,E',\vec{u}')$	Depth dependent density of inner excited electrons	S_a	Excitation function related to Auger processes
E'	Energy of the inner excited electron	$\vec{\kappa}$	Reciprocal lattice vector
$\vec{\kappa}'$	Wave vector of the inner excited electron	$\Gamma(q)$	Plasmon damping rate
		OPW	Orthogonalized plane wave
$\vec{u}'$	Momentum direction of the inner excited electron	ν	Band index
		$n_{[\vec{\kappa}]}$	Number of reciprocal lattice vectors of equal length
W	Surface barrier height		
E_F	Fermi energy	E_{max}	Upper integration limit in the transport equation
k_F	Fermi wave number		
Φ	Work function	q_c	Plasmon cut-off wave number
α'	Angle between the electron momentum and the outer normal of the surface	E_ν^a	Energetic position of the Auger excitation
α_c	Aperture of the escape cone	r_s	Mean interelectronic distance in Bohr units
$v(E)$	Electron velocity	$V_{\vec{\kappa}}$	Fourier coefficient of the model potential
$l(E)$	Total mean free path of the electron		
mfp	Mean free path	E_{nl}	Atomic energy level
$S(E_0;E',\vec{u}')$	Excitation function	a_B	Bohr radius
$W^\sigma(E',\vec{u}';E'',\vec{u}'')$	Transition function	L	Maximum escape depth
$R(E_0)$	Range of the primary electron	β	Efficiency of reflected electrons
$l^{el}(E)$	Elastic mean free path of the electron	$\vec{\kappa}_0$	Wave vector of the primary electron
		Θ	Excitation angle. Angle between $\vec{\kappa}_0$ and $\vec{\kappa}'$

possible to obtain SE signals with 1 nm spatial resolution and 1 eV energy resolution. In these considerations, the decay of plasmons will be assumed as the most important mechanism of SE generation. In a dedicated STEM, a high spatial resolution of 0.4 nm (for Al at an energy loss of 15 eV) and < 1 nm was achieved by Scheinfein et al. (1985) and by Bleloch (1989) and Bleloch et al. (1989), respectively. Two basic questions should be answered: first, what is the relative importance of the different processes by which SE are generated in the relevant region of primary energies used in the STEM, and secondly, what is the degree of localization of these generation processes in order to understand the high spatial resolution which happens in the experimental investigations. In the above mentioned calculations of the SEE for Al (Rösler and Brauer, 1991), it was shown that the generation of SE by plasmon decay leads to an important contribution to the total electron yield. If this holds in general, then the problem arises: how can we understand the high spatial resolution obtained in the experiment by excitation and decay of a primarily delocalized elementary excitation? The problem of localization in this case was discussed by Cheng (1987) using simple relations concerning the plasmon properties (dispersion, damping) in metals. A more elaborate but fundamental theoretical treatment, was given by Ritchie et al. (1990, 1991).

Independent of the explanation of the achievable spatial resolution related to the SE generation by plasmon decay, the problem remains: what is the role of different excitation processes depending on the primary energy with respect to the SE signal? From the experimental point of view, a new technique developed in recent years is suitable to decide this question. Measurements of energy-selected SE in coincidence with energy-loss events were performed by Pijper and Kruit (1991), Müllejans et al. (1991), Müllejans (1992) and Scheinfein et al. (1993). Different materials (C, Si, SiC, MgO) were investigated in the STEM at a primary energy of 100 keV. Unfortunately, there is no overlap between the materials and the primary energies used in the experiments and those for which calculations were performed. Therefore, it seems to be necessary to extend the calculations performed up to now for Al to other materials and higher primary energies. First calculations concerning the particle-induced electron emission from Mg and Be were performed by the author (Rösler, 1995) in order to obtain more general information about the effectiveness of different SE generation mechanisms, especially for proton impact. In the present paper, we will give a detailed description of the SEE of Mg and Be. As in the case of Al, we start from a transport equation formalism using the same basic models for the microscopic description of excitation and scattering

processes (Rösler and Brauer, 1991).

Basic Considerations Concerning the Description of SEE Within the Transport Equation Formalism

The number of electrons of energy E emitted per unit time and unit area of the surface in the direction $\vec{u}$, i.e., the energy and angle dependent current density $j(E,\vec{u})$ is the basic quantity in the description of SEE. $j(E,\vec{u})$ is normalized to the unit of current of PE with energy E_0 impinging on the surface. The maximum information about the emission process can be obtained by measuring this quantity. Usually, experimental results are given for the energy distribution of emerging electrons

$$j(E) = \int j(E,\vec{u})d\Omega \qquad (1)$$

and the electron yield

$$\sigma = \int_0^{E_0} j(E)dE = \int_0^{50} j(E)dE + \int_{50}^{E_0} j(E)dE = \delta + \eta \qquad (2)$$

The spectrum of outgoing electrons contains, besides the contribution of "true" SE δ, the contribution of backscattered electrons η. As usual, the value of 50 eV is chosen for the separation of both types of emitted electrons. The yield of true SE δ is given by the contribution of incident (δ_0) and backscattered PE.

The energy and angular dependent current density of emerging electrons $j(E,\vec{u})$ can be obtained from that part of the current density of inner excited electrons $j_i(E',\vec{u}')$ containing all electrons which fulfill the escape conditions. For the description of the escape of excited electrons, we use the standard model of a planar surface barrier and free electrons inside the metal (Brauer, 1972). From the conservation laws for energy and parallel momentum of the electrons, we obtain the relation between outer $(E,\vec{u})$ and inner $(E',\vec{u}')$ variables. The usual conditions which are necessary for the escape of an electron $(E',\vec{u}')$ are given by (Brauer, 1972; Rösler and Brauer, 1991; Rösler, 1994a).

$$E' > W$$
$$\cos\alpha' > \cos\alpha_c = \sqrt{\frac{W}{E'}} \qquad (3)$$

α_c defines the so called escape cone. It is the maximum emission angle at which the normal component of the momentum is sufficient for the electron to surmount the surface barrier. The surface barrier W is determined in

metals by the Fermi energy E_F and the work function Φ:
$W = E_F + \Phi$.

The current density of inner excited electrons $j_i(E',\vec{\Omega}')$ is given by the density of inner excited electrons at the surface $N(E',\vec{\Omega}') = N(x = 0,E',\vec{\Omega}')$ (Rösler and Brauer, 1991). $N(x,E',\vec{\Omega}')$ can be obtained by solution of the Boltzmann transport equation taking into account the boundary conditions at the surface (Puff, 1964; Rösler, 1994a).

The spatial dependence of the problem is related to the restriction on the half space as well as to the spatial dependence of the excitation rate. If we restrict ourselves to primary energies above 1 keV, then the range $R(E_0)$ of impinging monoenergetic PE is larger than the maximum escape depth L of SE. Then, the assumption of a homogeneous excitation of SE in the layer below the surface which is relevant for the emission process is justified. Nevertheless, also in this case, the spatial dependence of the transport problem is determined by the boundary conditions at the surface (Puff, 1964). It is shown by Devooght *et al.* (1992) using a simplified description of the scattering properties, that the solution of the homogeneous transport equation

$$\frac{v(E')}{l(E')}N(E',\overline{\Omega}') = S(E_0;E',\overline{\Omega}') +$$
$$\int\int dE''d\Omega''W^\sigma(E',\overline{\Omega}';E'',\overline{\Omega}'')N(E'',\overline{\Omega}'') \quad (4)$$

taking into account the escape conditions (Eq. 3) {so-called infinite-slowing-down (ISD) model} overestimates the number of excited electrons by nearly 25% compared with the correct solution of the half space problem including the boundary conditions at the surface. Nevertheless, we will use the ISD model in the following in order to reduce the numerical effort. In (Eq. 4), $v(E)$ and $l(E)$ denote the speed and the total mean free path (mfp) of the electron, respectively. The primary energy dependent excitation function $S(E_0;E,\vec{\Omega})$ expresses the number density of electrons in the state $k'(E',\vec{\Omega}')$ created per unit time and per unit energy by the PE. This function is normalized to unit primary current. The second term on the right hand side of (Eq. 4) denotes the number of electrons scattered into the state $k'(E',\vec{\Omega}')$ by collisions. This number is determined by the so-called transition function W^σ. The left hand side of (Eq. 4) expresses the number of electrons scattered out of the state $k'(E',\vec{\Omega}')$. Both quantities, the total mfp and the transition function, include elastic as well as inelastic scattering processes (Rösler and Brauer, 1991).

$$\frac{1}{l(E)} = \frac{1}{l^{el}(E)} + \frac{1}{l^{inel}(E)} \quad (5)$$

As usual, the angular dependence of the problem will be treated by expansion into Legendre polynomials P_l. According to the separation into elastic (el) and inelastic (inel) scattering processes, the expansion coefficient of the transition function can be written as

$$W_l^\sigma(E',E'') = W_l^{(el)}(E',E'') + W_l^{\sigma(inel)}(E',E'') \quad (6)$$

In order to simplify the explicit calculations of the SEE for Mg and Be, we will restrict ourselves to perpendicular incidence of PE. Most of the experiments were carried out on polycrystalline targets. Therefore, a restriction to such targets is reasonable. The input parameters which are used in the evaluation of scattering properties as well as the excitation rates in the next section, are collected in Table 1.

In Figure 1, the different contributions to the total mfp are shown for Al, Mg, and Be. The inelastic mfp's were calculated within the free-electron-gas picture in random phase approximation (RPA) (Quinn, 1962). Local field corrections which modify the RPA result have been neglected. In the description of the transport of inner excited electrons, we leave out the contribution to the inelastic mfp as well as to the scattering function determined by the interaction with core electrons. For the lowest primary energies considered here, this assumption is well justified. However, with increasing primary energy, there is a larger number of SE with higher excitation energies. For these electrons, scattering processes with participation of core electrons gain in importance. Nevertheless, in order to reduce the numerical effort in the calculations, we will neglect these contributions to the scattering quantities.

Besides the different inelastic scattering processes, elastic scattering should be taken into account in the description of transport of inner excited electrons. This type of scattering is of special importance provided that the excitation mechanism in question leads to an anisotropic distribution of excited electrons. The problems, which are related to the evaluation of the elastic cross-sections, are extensively discussed by Devooght *et al.* (1991). The elastic cross-sections can be obtained by the partial wave expansion method (PWEM) using suitable atomic potentials within a muffin tin scheme. For Al, reliable results for the elastic scattering cross-sections and therefore, for the corresponding elastic mfp and scattering functions are available (Rösler and Brauer, 1991; Devooght *et al.*, 1991). They were obtained using the muffin tin potentials given by Smrčka (1970) or by an improved version of the computer program given by Pendry (1974). In the case of Mg and Be, the elastic mfp shown in Figure 1b as well as the elastic scattering function $W^{(el)}$, were obtained by the PWEM using the computer program given in (Pendry, 1974).
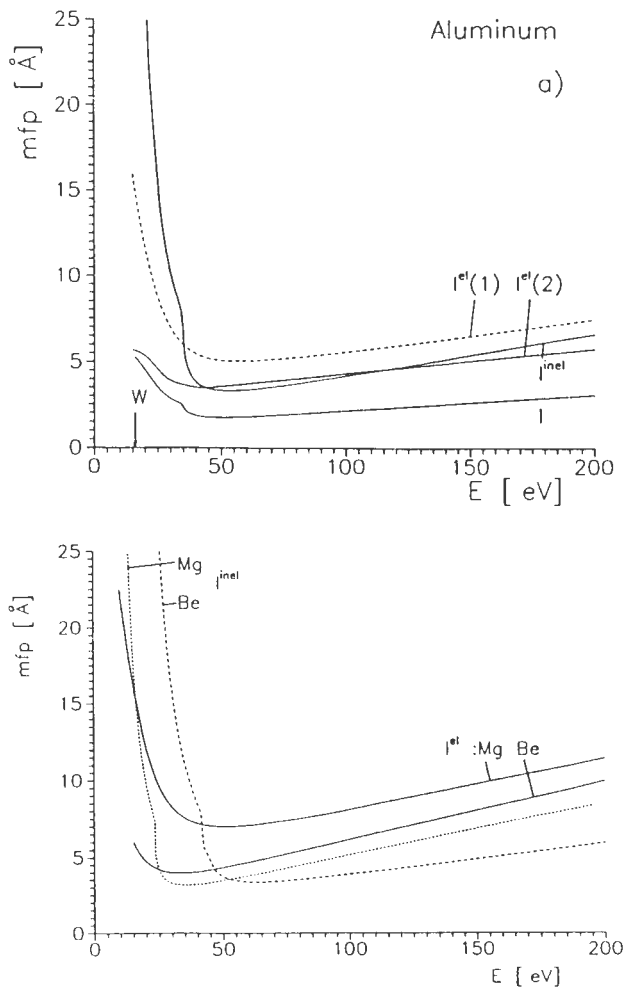
Figure 1. Calculated mean free paths (mfp) of electrons in Al (**a**), Mg, and Be (**b**) as a function of energy, measured from bottom of conduction band. l^{el}, l^{inel}, and l denote the elastic, inelastic, and the total mfp, respectively. The arrow indicates the vacuum level. For Al (**a**), the elastic mfp's obtained from the computer program given by Pendry (1974) $l^{el}(1)$, as well as $l^{el}(2)$ obtained by the PWEM using Smrčka's (1970) muffin tin potential are shown (see text).

With respect to the magnitude of the elastic and inelastic mfp, we obtain for Al and Be (Figs. 1a and 1b) nearly the same behavior, whereas for Mg (Fig. 1b), the elastic mfp is distinctly larger than the inelastic one. In this connection, a short comment is appropriate. In Figure 1a, we have plotted for Al, both the elastic mfp obtained from the improved phase shift calculation mentioned above, and the elastic mfp obtained from the computer program given in (Pendry, 1974), which was used here for Mg and Be. This latter mfp is larger than the first one in the whole energy range. We expect a considerable reduction of the mfp in the case of Mg and

Be if we take into account the same improvements concerning the atomic potentials used in the phase shift calculations as for Al. Preliminary results for the elastic mfp's for both metals obtained from the phase shifts calculated by Heinz (personal communication, 1995) using an improved computer program confirm this expectation.

Excitation Processes

The interaction between the PE and the electron system of the metal leads to different possibilities of generating SE. We will restrict ourselves in the following to the same basic excitation mechanisms considered already in the description of the SEE of Al (Rösler and Brauer, 1991). Four different excitation processes should be taken into account. First, there are processes which are related to the conduction band: (i) excitation of single conduction electrons (S_e), (ii) excitation of conduction electrons by the decay of plasmons generated by the PE (S_p). Secondly, in a complete description of the emission phenomenon, inner shell ionization processes should be taken into account. Besides the direct excitation of core electrons by the impinging PE (S_c) there is the delayed process via Auger processes (S_a). This Auger process follows immediately the creation of the inner shell vacancies by the PE. We will restrict ourselves to Auger processes with participation of the conduction band.

The excitation of conduction electrons by decay of surface plasmons generated by the impinging PE will be neglected. With respect to the total number of excited electrons, this excitation mechanism is of minor importance compared with the other excitation processes, especially in the case of perpendicular incidence considered in this paper (Chung and Everhart, 1977).

The basic formulas for the evaluation of the different excitation rates can be found in (Rösler and Brauer, 1981a,b, 1991; Rösler, 1994a). With exception of the excitation by Auger processes, the other excitation functions can be obtained from a golden rule expression for the transition probability between Bloch states for two interacting point charges. In every case, this expression can be simplified by the assumption that the PE before and after the scattering event is in a plane wave state. In the case of excitation via Auger processes, a simple model was proposed by Rösler and Brauer (1991) and Rösler (1991). Some comments are useful with respect to the evaluation of the different excitation functions.

Excitation of single conduction electrons S_e

In the case of excitation of single conduction electrons the free-electron-gas model is appropriate. The screening of the electron-electron interaction will be described by the Lindhard or RPA dielectric function. It was shown in Rösler and Brauer (1991), that for high
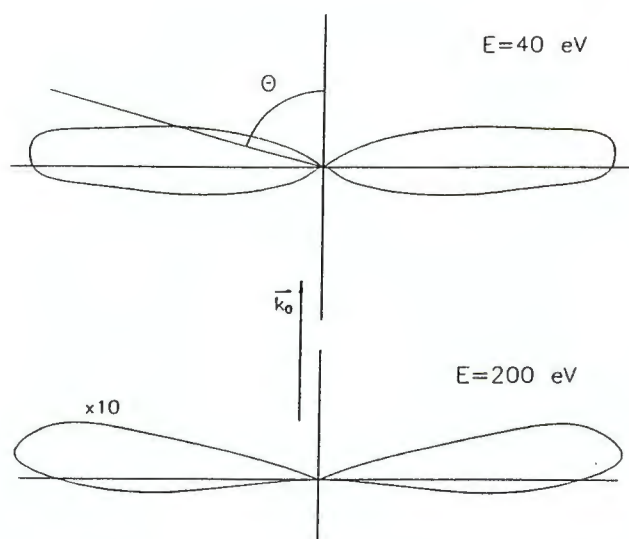
Figure 2. Angular dependence of the excitation of single conduction electrons for Be at E = 40 and 200 eV. E_0 = 20 keV. $\vec{K}_0$ denotes the wave vector of the primary electron and Θ is the excitation angle.

---

excitation energies ($E_0 \gg \hbar\omega_p$, ω_p is the plasma frequency at zero wave number) screening is unimportant and the excitation rate approaches the excitation function first derived by Streitwolf (1959). At lower excitation energies, dynamic screening should be taken into account. Thomas-Fermi screening underestimates the excitation rate at all secondary energies (Rösler and Brauer, 1991). With respect to the shape of the energy and angular distribution of inner SE, we obtain qualitatively the same behavior as for Al. At low primary energies (of order 1 keV), the excitation takes place nearly perpendicular to the direction of the primary beam. With increasing excitation energy, we observe an increased tendency of the excitation in the inward direction as can be seen in Figure 7.10 in Rösler and Brauer (1991). At high primary energies (of order 20 keV), the excitation takes place in a small angular region around the direction perpendicular to the primary beam for all excitation energies. This can be seen in Figure 2 for Be.

Excitation of conduction electrons by decay of bulk plasmons S_p

In RPA there is no damping of bulk plasmons for small wave numbers. Therefore, in order to calculate the excitation function related to the decay of plasmons generated by the PE, it is necessary to go beyond the simple RPA description of the free-electron-gas model. To do this, there are two possibilities. First, within the free-electron-gas picture, plasmon decay happens only by higher order processes with respect to the Coulomb

interaction, e.g., by creation of two electron-hole pairs (Sturm, 1982; Bachlechner, 1994). However, the magnitude of the plasmon damping found in the experiments (see Table 1) cannot be explained by this or other higher order processes. Secondly, a finite plasmon damping, especially at small wave numbers, can be obtained taking into account the real energy band structure. It was shown by Paasch (1969) and later on by Sturm (1976, 1977, 1982) that in NFE metals the plasmon damping is determined to a great extent by interband processes (for polycrystalline metals, a further plasmon damping mechanism is important: it was shown by Krishan and Ritchie (1970) that decay of volume plasmons into single particle states may proceed by scattering on inhomogeneities (grain boundaries); we will neglect this additional excitation mechanism). The same type of interband processes which govern the plasmon damping are responsible for the excitation of conduction electrons into states which belong to higher unoccupied energy bands (Chung and Everhart, 1977; Rösler and Brauer, 1981a,b, 1991; Rösler, 1994a,b).

In NFE metals, the band structure can be described within a model potential scheme. Electron wave functions and Bloch energies can be obtained by perturbation theory with respect to this weak model potential. Transition matrix elements which appear in the excitation function as well as the energy bands, especially their behavior in the vicinity of the zone boundaries, can be obtained with sufficient accuracy by perturbation theory for nearly degenerate states (two-band model). In order to obtain a formula which is applicable to polycrystalline targets, an average over all directions of the reciprocal lattice vectors was performed (Rösler and Brauer, 1981a). In this way, the contributions of the different interband processes are given by this average multiplied by the number of reciprocal lattice vectors of equal length $n_{[\vec{k}]}$ given in Table 1.

The evaluation of the excitation rate by plasmon decay requires as an input quantity the total wave number dependent plasmon damping rate $\Gamma(q)$ including all mechanisms (interband transitions, higher order effects beyond RPA, core polarization effects) which determine this quantity (Sturm, 1982). In order to restrict the numerical effort to an acceptable scope, the use of the measured plasmon damping rate in the calculation procedure (Rösler and Brauer, 1991) seems to be justified for our purpose. According to Kloos (1973) and Krane (1978), the experimental results for the plasmon damping in Al and Mg can be written as $\Gamma(q) = \Gamma_0 + \Gamma_2(q/k_F)^2$. The values obtained from the measurements are given in Table 1. For Be, there are no corresponding results. From the measurements by Eisenberger et al. (1973) the value Γ_0 can be obtained by extrapolation (see Table 1).

Table 1. Input quantities used in the calculations. The experimental plasmon damping can be written as $\Gamma(q) = \Gamma_0 + \Gamma_2(q/k_F)^2$. Γ_0 for Be can be obtained from the values given by Eisenberger and Platzman (1973) by extrapolation. The values of the Fourier coefficients of the model potential are given by Animalu and Heine (1965) for Al and Mg, Cohen and Heine (1970) for Mg, and Ashcroft (1968) for Be. The position of the Auger excitation E_ν^a is measured from bottom of conduction band.

	Al	Mg	Be
lattice structure	fcc	hcp	hcp
lattice constant [A]	a = 4.040	a = 3.203 c/a = 1.620	a = 2.281 c/a = 1.568
r_s	2.08	2.65	1.866
E_F [eV]	11.6	7.14	14.4
$\hbar\omega_p(0)$ [eV]	15.6	10.9	18.5
work function Φ [eV]	4.30	3.70	4.98
$V_{\vec{K}}$ [eV] Mg: Cohen and Heine (1970) Be: Ashcroft (1968) $V_{\vec{K}}$ [eV] Al and Mg: Animalu and Heine (1965)	 $V_{[111]} = 0.243$ $V_{[200]} = 0.764$	$V_{[1010]} = 0.190$ $V_{[0002]} = 0.354$ $V_{[1011]} = 0.490$ $V_{[1012]} = 0.789$ $V_{[1012]} = 0.547$	0.925 1.278 1.306 0.870
$n_{\vec{K}}$	$n_{[111]} = 8$ $n_{[200]} = 6$	$n_{[1010]} = 6$ $n_{[0002]} = 2$ $n_{[1011]} = 12$ $n_{[1012]} = 12$	6 2 12 12
plasmon damping, (exp): Γ_0, Γ_2 in [eV]	0.5 3.0	0.7 2.14	2.,..4. 0
plasmon cutoff wave- number: q_c/k_F (RPA)	0.7395	0.8105	0.7101
binding energies: (measured up to the Fermi level) in [eV]	$E_{2s} = 117.6$ $E_{2p} = 72.6$	87.14 52.14	$E_{1s} = 111.0$
Auger excitation: position in [eV]	$E_{2p}^a = 82.9$	55.8	$E_{1s}^a = 115.0$

Notes on Table 1: Compared with the table of input parameters given in Rösler (1995), we have included the values for the numbers of equivalent reciprocal lattice vectors $n_{\vec{K}}$ as well as for Mg the Fourier coefficient $V_{\vec{K}}$ obtained from the model potential of Heine and Abarenkov (Animalu and Heine, 1965). For Mg, the Fourier coefficients $V_{\vec{K}}$ with $i \leq 3$ are nearly the same for the different model potentials as can be seen in Figure 14. We have used both model potentials (Heine and Abarenkov, Cohen and Heine) in order to calculate the $\vec{K}_4$-contribution to the excitation function S_p (see Fig. 3a).
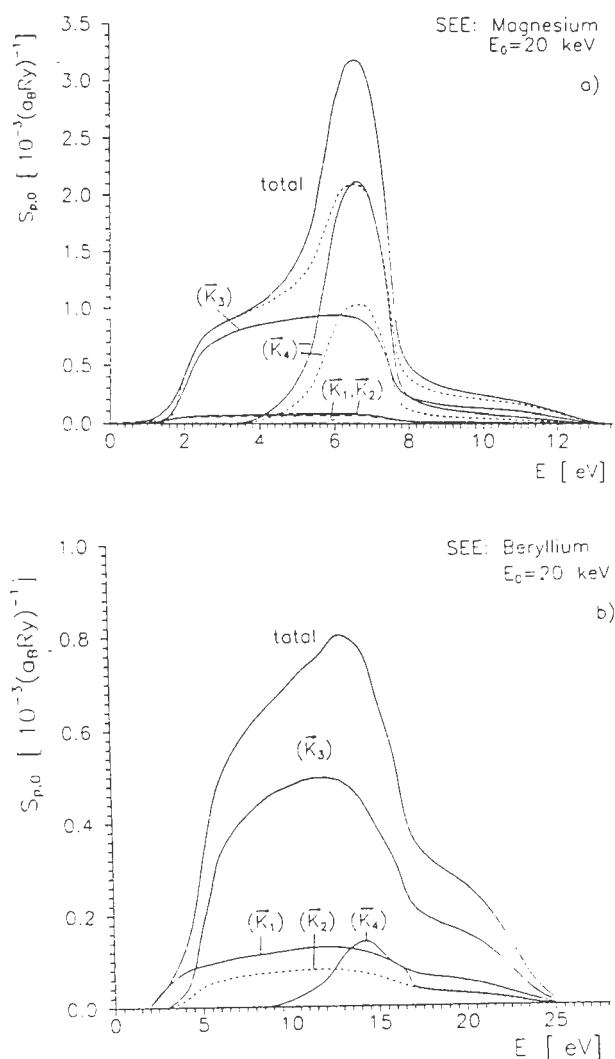
Figure 3. Energy distribution of the excitation by plasmon decay for polycrystalline Mg (a) and Be (b) at E_0 = 20 keV. Decomposition of the total excitation rate into the contributions from different interband transitions denoted by the corresponding reciprocal lattice vectors $\vec{K}_i$ (i = 1,... 4). For Be, we have used Γ_0 = 4 eV and Γ_2 = 0 in the calculations. For Mg, the dashed lines denote the $\vec{K}_4$-contribution as well as the total excitation function using the model potential of Heine and Abarenkov (see Table 1).

The excitation function consists of the contributions of the different interband processes which can be labeled in an extended zone scheme by the corresponding reciprocal lattice vectors $\vec{K}_i$ (i ≤ 3 for Al, i ≤ 4 for Mg and Be). In Figure 3, a comparison of the contributions from the different interband transitions to the energy distribution of the total excitation rate S_p is shown for Mg and Be for E_0 = 20 keV. Compared with lower pri-

mary energies {for E_0 = 2 keV (Rösler, 1995)}, there is no change in the general behavior of the different components of the excitation rate. The magnitude of the different contributions is directly related to the magnitude of the corresponding model potential Fourier coefficients given in Table 1. It should be noted that for both metals the contributions from the interband transitions related to $\vec{K}_1$ = $\vec{K}_{[10\bar{1}0]}$ and $\vec{K}_2$ = $\vec{K}_{[0002]}$ are of minor importance. In the case of Mg, the contributions resulting from the $\vec{K}_3$- and $\vec{K}_4$-processes are comparable in magnitude. However, the behavior of the $\vec{K}_4$-interband transition leads in the total excitation rate to a sharp decrease of the energy distribution at an energy approximately given by $\hbar\omega_p$-Φ. In the case of Be, the $\vec{K}_4$-contribution is reduced compared with the $\vec{K}_3$-contribution. Therefore, the energy distribution of the total excitation rate S_p for Be shows a moderate decrease on the high energy side.

Using the model potential of Heine and Abarenkov (see Table 1), there is, in the case of Mg, a distinct reduction of the $\vec{K}_4$-contribution as shown in Figure 3a. This behavior leads to a reduction of the contribution of the excitation by plasmon decay to the emission properties compared with the excitation rate obtained with the model potential of Cohen and Heine. In the calculations we have used this latter model potential (see Table 1).

In Figure 4, the energy distribution of the total excitation rate S_p is shown for Mg and Be for two different primary energies. With respect to the primary energy dependence, there is no substantial change in the behavior if we go from E_0 = 2 keV to e.g., 20 keV. In every case, the excitation rate is governed by the energy transfer $\hbar\omega_p$(q ≈ 0) to the system of conduction electrons. Effects of the plasmon dispersion which can be seen in the case of proton induced KEE for Al and Mg at low impact energies (Rösler, 1994a,b) should be important in the case of SEE for primary energies below ~ 100 eV. However, for such low primary energies our theory which is based on the ISD model is not applicable as mentioned above.

Comparing the behavior of the energy distribution of S_p for the different metals, we obtain for Al (see Rösler and Brauer, 1991) and Mg that the strong decrease of the excitation rate on the high energy side leads to a distinct structure in the energy distribution of emerging electrons. This so-called plasmon-shoulder is clearly seen in the measured spectra obtained from clean targets (Jenkins and Chung, 1972). For Be, we obtain no such feature by reason of the moderate decrease of the excitation rate on the high energy side mentioned above. The measured spectra in the case of SEE (Koshikawa and Shimuzu, 1974), as well as in the case of proton-induced KEE (Hippler, 1988), show also no plasmon shoulder.
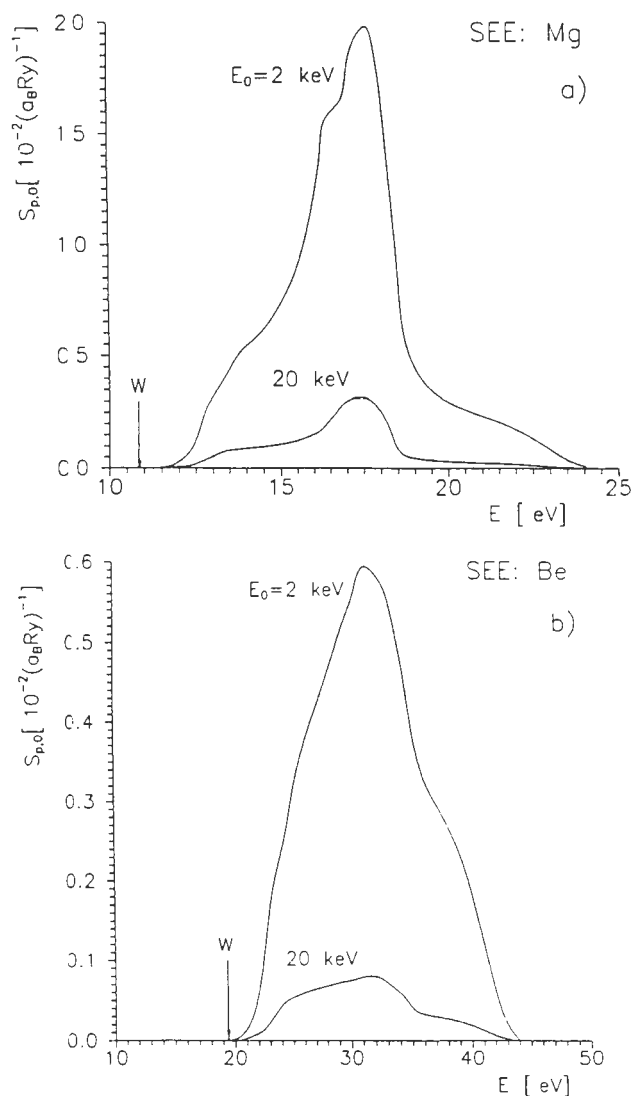
Figure 4. Energy distribution of the excitation by plasmon decay for polycrystalline Mg (a) and Be (b) for different primary energies (E_0 = 2 and 20 keV). For Be, we have used Γ_0 = 4 eV and Γ_2 = 0.

It is interesting to consider the angular dependence of the excitation by plasmon decay. In Figure 5, this angular distribution is shown for Mg and Be at low and medium primary energy. The excitation energy is chosen in every case nearly at the maximum of the excitation rate. As in the case of Al (Rösler and Brauer, 1991), the excitation shows a distinct angular dependence. However, compared with Al, there is, in both cases, a larger excitation rate in the backward direction.

Direct excitation of core electrons S_c

There are different methods of calculating the excitation of core electrons. Within an atomic picture, the ionization of inner shells can be described by the semi-
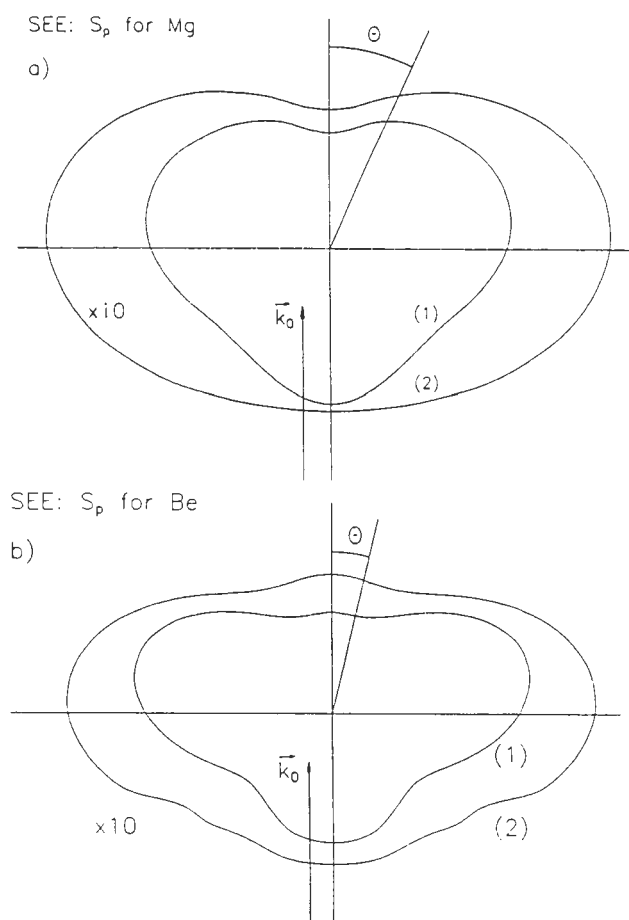

Figure 5. Angular dependence of the excitation of conduction electrons by plasmon decay at different primary energies {2 keV (1) and 20 keV (2)} for Mg (a) and Be (b). The excitation energies are: 7 eV for Mg and 12 eV for Be (measured from the vacuum level). $\vec{K}_0$ denotes the wave vector of the primary electron. Θ is the excitation angle.

----

classical model of Gryzinski (1965a,b,c) or, according to Tung and Ritchie (1977), from the atomic generalized oscillator strengths calculated by Manson (1972). In the first case, we have a simple analytical formula for the differential cross-section for an energy transfer ΔE from the PE to an electron in a core state. This formula can be used with benefit in all Monte-Carlo calculations of SEE.

In our approach, the crystal electrons are described within a Bloch scheme: the core states and excited states of electrons are given by so-called Bloch sums and orthogonalized plane waves (OPW), respectively. Bloch sums are linear combinations of atomic wave functions centered on different lattice points. This calculation procedure works very well if overlap integrals between
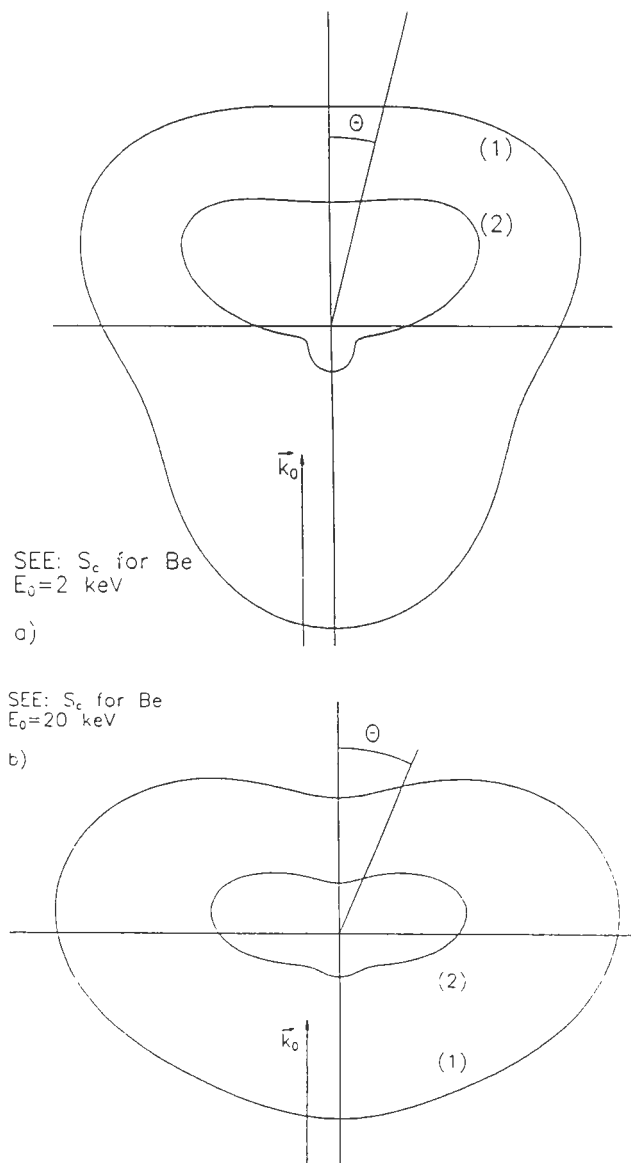
Figure 6. Angular dependence of the excitation of core electrons in Be for different primary energies (E_0 = 2 and 20 keV) at different excitation energies: 50 eV (1) and 200 eV (2) (measured from bottom of conduction band). $\vec{K}_0$ denotes the wave vector of the primary electron, and Θ is the excitation angle.

----

atomic functions at neighbouring lattice points are small (Rösler and Brauer, 1981a,b). Nevertheless, the excitation rate can be calculated only with considerable numerical effort.

If we compare the energy dependent excitation function for the Gryzinski model and our OPW calculation, remarkable differences are obvious. With our model, we obtain a larger number of SE with higher energies, whereas at low secondary energies, our excitation rate

is distinctly below the excitation rate obtained from the Gryzinski model. This behavior can be found for all three metals considered here {for Al, see also Rösler and Brauer (1991)}.

With respect to the angular dependence of the excitation, we obtain for Mg and Be qualitatively the same behavior as for Al (Rösler and Brauer, 1991). This can be seen in Figure 6 for Be for E_0 = 2 and 20 keV at low and high excitation energies. At low excitation energies, the excitation is nearly isotropic, whereas with increasing energy, the excitation takes place preferably in the forward direction, especially at low primary energies.

The core states are labeled by the index ν. The Bloch energies are approximately given by the corresponding atomic levels: $E_{\vec{K}\nu} \approx E_\nu = E_{nl}$. In the case of Al and Mg, we will only take into account the excitation of L-shell (ν = 2p, 2s) electrons. Due to the large binding energy of the 1s-electron, the excitation from the K-shell will be neglected. For Be, we have ν = 1s. The corresponding binding energies are given in Table 1. In actual calculations, Herman-Skillman functions (Herman and Skillman, 1963) are used for the radial part of the atomic wave functions.

Excitation of conduction electrons via Auger processes S_a

Here we are not interested in the details of the emission spectra in the region of the Auger energies of the target material. With respect to our investigation of the SEE features at low energies, we are interested in the role of the more or less monoenergetic isotropic excitation of conduction electrons by Auger processes at energies which are related to the binding energies of the different atomic core levels. For that purpose, it is sufficient to use the simple three or two parameter model proposed by Rösler (1991); Rösler and Brauer (1991).

The basic assumption in this model is that the vacancies created by the impinging PE in the inner shells by direct excitation of core electrons are immediately filled within a very short time ($\leq 10^{-12}$ sec) by electrons from higher occupied levels. The strength of this excitation is determined by the basic assumption that the number of electrons excited by Auger processes is equal the number of excited core electrons or inner shell vacancies produced by the PE (Rösler, 1991; Rösler and Brauer, 1991). This condition can be written as

$$\int \int S_c^\nu(E_0;E,\overline{\Omega})\,dE\,d\Omega =$$
$$4\pi \int S_a^\nu(E_0;E)\,dE = \frac{1}{l_\nu^{inel}(E_0)} \qquad (7)$$

Therefore, the strength of excitation with participation of the core state ν is related to the contribution of this core state to the inelastic mean free path $l^{inel}(E_0)$.
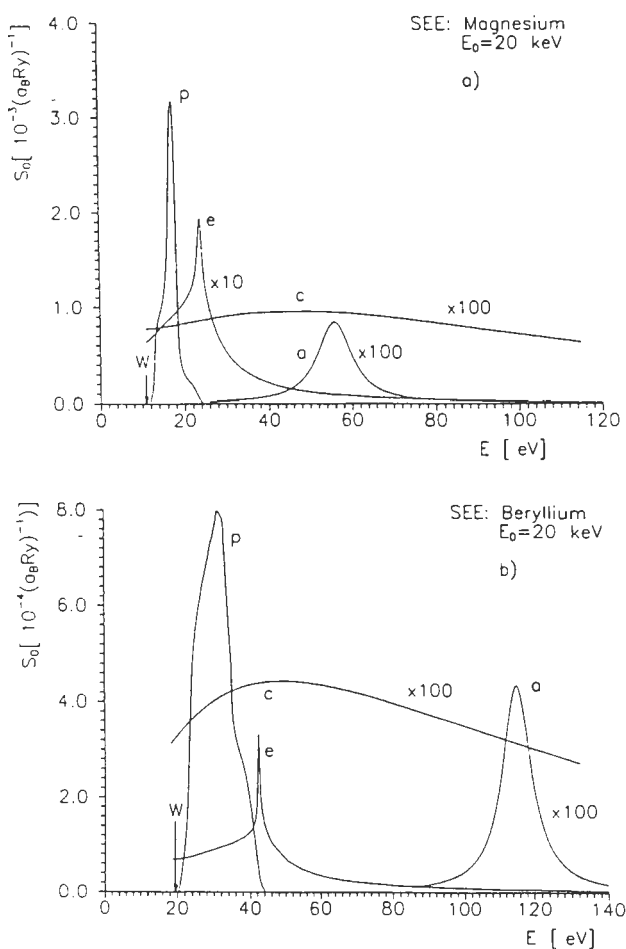
Figure 7. Energy dependence of different excitation functions for Mg (a) and Be (b) at high primary energy (E_0 = 20 keV). Excitation by decay of plasmons (p), of single conduction electrons (e), of core electrons (c), and by Auger processes (a). The arrow indicates the vacuum level.

Comparison of different excitation mechanisms

All excitation processes discussed above occur simultaneously. Therefore, a comparison of the different excitation rates should be useful. The first term (l = 0) of the expansion of the excitation function $S(E_0;E,\vec{n})$ into Legendre polynomials defines the energy dependent excitation function $4\pi S_{l=0}(E_0;E)$. In Figure 7, the different energy dependent excitation functions are shown for Mg and Be at E_0 = 20 keV. Qualitatively, the same behavior was obtained as for Al (Rösler and Brauer, 1991). However, there are changes in the relative magnitude of the different excitation rates. It is hardly possible to make statements about the importance of the different excitation mechanisms for the emission phenomenon. Whereas S_p and S_a are restricted on finite energy intervals at relatively low energies, the other excitation

mechanisms S_e and S_c create excited electrons up to energies $\leq E_0$. In general, the excitation of core electrons is the dominant excitation mechanism at high excitation energies whenever the number of core electrons exceeds the number of conduction electrons. The number of electrons excited by this mechanism exceeds the number of directly excited conduction electrons above 100 eV (Al) and 85 eV (Mg) for E_0 = 1 keV and above 65 eV (Al) and 55 eV (Mg) for E_0 = 20 keV. This would be essential with respect to the enhanced effectivity of energetic electrons via the electron cascade. For Be, the relation between these two excitation mechanisms is slightly different compared with Al and Mg. At low primary energies (E_0 = 1 keV), the number of electrons excited from the 1s-level is smaller than the number of conduction electrons excited directly by the PE in the whole energy range. At higher primary energies, S_c gains in importance. For instance, for E_0 = 20 keV, the number of electrons excited from the 1s-level exceeds the number of directly excited conduction electrons above 225 eV.

Solution of the Transport Equation

The expansion of the angular dependent quantities in (Eq. 4) with respect to Legendre polynomials P_l leads to a set of independent integral equations (for l = 0,1,...)

$$\frac{\nu(E')}{l(E')}N_l(E') =$$

$$S_l(E_0;E') + \int_E^{E_{max}} dE'' W_l^\sigma(E',E'')N_l(E'') \tag{8}$$

where N_l, S_l, and W_l^σ are the expansion coefficients of the density of inner excited electrons, the excitation function, and the scattering function, respectively. In a first attempt, a restriction to $l \leq 2$ is sufficient (Rösler, 1993).

In general, the upper limit of the energy integration in (Eq. 8) is given by the primary energy E_0. However, depending on the special features shown by the different excitation functions (see Fig. 7), we can use an upper limit E_{max} which is distinctly below E_0. In the case of excitation by plasmon decay, the upper border of excitation energies is given by the plasmon energy and the plasmon damping at the cut-off wave number q_c (given in Table 1). In this way, we obtain from $E_{max} \approx \hbar\omega_p(q_c) + \Gamma(q_c) + E_F$: $\approx$ 37 eV for Al, $\approx$ 26 eV for Mg, and $\approx$ 46 eV for Be. In the case of excitation via Auger processes, the upper border of excitation energies is given by the position of the Auger excitation E_r^a and the width of the chosen initial energy distribution of the excitation rate $\{S_a{}'(E_0;E) = A_r(E_0)\delta(E-E_r{}^a)$ or a broadened distribution, Rösler (1991), Rösler and Brauer
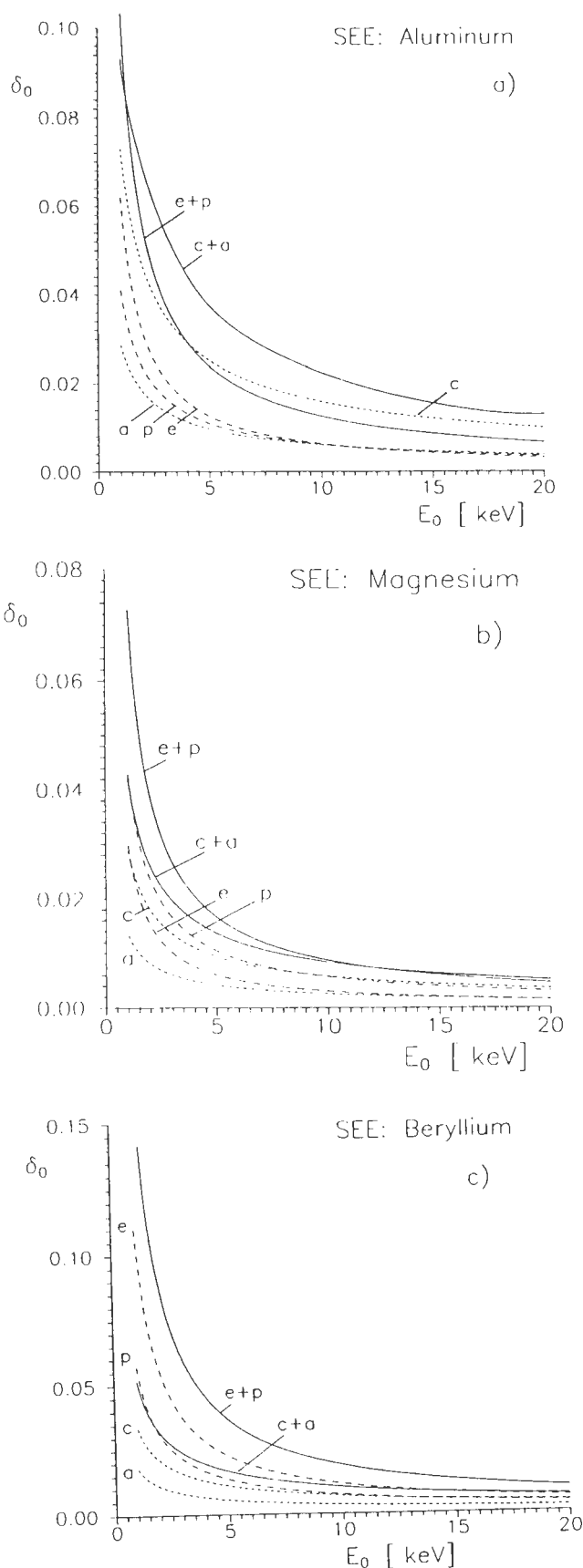
Figure 8. Primary energy dependence of the electron yield δ_0 for Al (a), Mg (b), and Be (c). Contributions of the different excitation mechanisms: excitation of single conduction electrons (e), by decay of plasmons (p), of core electrons (c), and by Auger processes (a). Contributions from different groups of excitation processes: (e + p) excitation processes restricted to the conduction band, (c + a) excitation restricted to processes with participation of core states.

(1991)}. For both types of excitation, E_{max} is independent of the primary energy.

In the case of excitation of single conduction and core electrons (S_e, S_c), SE will be generated up to high excitation energies (see above, **Excitation Processes**). Then, the strength of decrease of the excitation rate with increasing excitation energy determines the value of E_{max}. In our calculations we have used, for simplicity in every case, $E_{max} \approx 900$ eV. It can be shown that for high primary energies higher values of E_{max} should be used, especially in the case of excitation of core electrons, because for this excitation mechanism there is an enhanced number of excited electrons with energies in the keV range. These energetic electrons are most effective with respect to the generation of low energy electrons by scattering processes within the system of target electrons.

Results for the Electron Yield δ_0.
Comparison with Experimental Data

Within the transport equation formalism, we obtain from the solution of (Eq. 4) or (Eq. 8) only that part of the density of inner excited electrons which results directly from the interaction of the PE with the system of target electrons. The corresponding contribution of the electron yield will be denoted by δ_0 (see above, **Basic Considerations Concerning the Description of SEE Within the Transport Equation Formalism**).

In Figure 8, we compare for Al, Mg, and Be the contributions of the different excitation rates to the electron yield in the range of primary energies from 1 to 20 keV. Compared with Al there are, for Mg and Be, some differences in the relative importance of the various excitation mechanisms. With respect to the results for Al, published up to now, there are improvements in the calculation of the contributions related to the direct excitation of single conduction electrons and core electrons by extending the cut-off energy E_{max} in (Eq. 8) to higher values (see below, **The Role of Different Scattering Processes**). Nevertheless, the statements obtained for Al concerning the relative importance of the different excitation mechanisms should be valid as ever
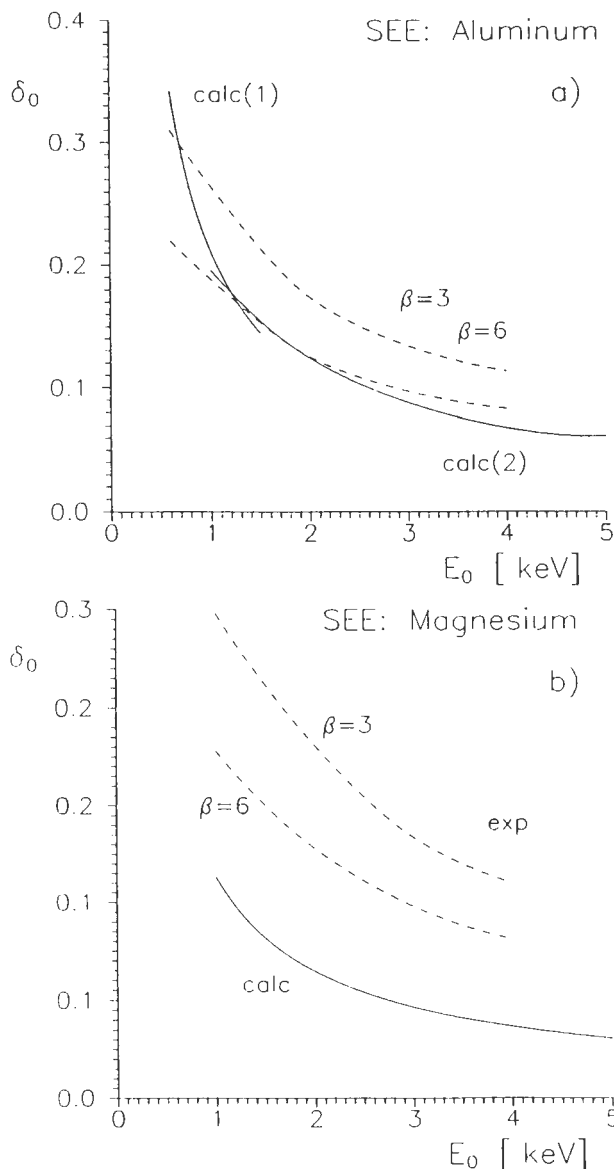
Figure 9. Primary energy dependence of the electron yield δ_0 for aluminum (a), magnesium (b), and beryllium (c). Comparison of experimental and theoretical results for primary energies below 4 keV. The dashed curves for different values of the efficiency β of reflected electrons render the probable range of experimental δ_0 values (see text). For aluminum (a), calc(1) denotes the theoretical results obtained by Bindi *et al.* (1980), and calc(2) denotes our own results.

(Rösler and Brauer, 1995). With increasing primary energy, the contribution to the yield δ_0 related to inner shell excitations (c + a) is distinctly larger than the contribution related to the excitation of conduction electrons (e + p) (see Fig. 8a).

For Mg, the contribution of the excitation of conduction electrons by plasmon decay is the dominant excitation mechanism at low primary energies (Rösler, 1995). Compared with the yield contribution related to the excitation of conduction electrons (e + p), which is the most important contribution at low primary energies, the contribution related to the excitation of inner shell electrons (c + a) gains in importance with increasing primary energy (see Fig. 8b).

For Be, the excitation of single conduction electrons S_e is the most important excitation mechanism in the whole range of primary energies (Rösler, 1995). The

contribution to the electron yield related to inner shell excitations (c + a) is distinctly below the contribution related to the excitation of conduction electrons (e + p) (see Fig. 8c).

In Figure 9, a comparison of our calculated yields with the experimental data is given. Unfortunately, there are no actual measurements of the emission properties in the case of SEE under definite statements about the quality of the target surface {a critical discussion of older experimental data is given by Seiler (1967)}. Therefore, with respect to the comparison of our calculated results with the experimental ones, some care is advisable. Moreover, the experimental data for the yield δ of true SE as well as for δ_0 given by Bronshtein and Fraiman (1969) are restricted to primary energies $\leq$ 4 keV. The measurements by Bindi *et al.* (1980b) are restricted to primary energies $\leq$ 1.5 keV. δ_0 can be obtained from the measured yield δ of true SE according to $\delta_0 = \delta/(1 + \beta\eta)$ (Seiler, 1983). For the yield of backscattered electrons η, we have used the fit formula given by Staub (1994). At present, there are no reliable statements about the efficiency β of reflected electrons. For this reason, we have used for β the limiting values given by Bronshtein and Fraiman (1969) for the restricted interval of primary energies shown in Figure 9.
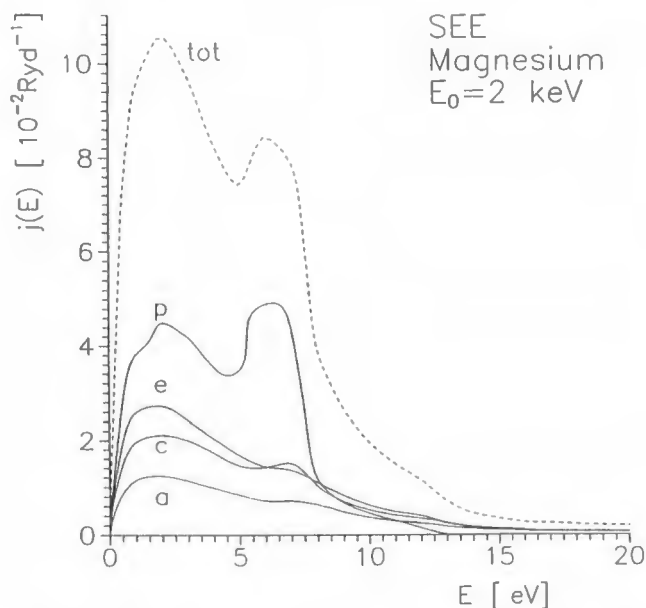
Figure 10. Energy distribution of SE for Mg. Contributions from different excitation mechanisms: excitation of single conduction electrons (e), by decay of plasmons (p), of core electrons (c), and by Auger processes (a); tot = total. $E_0 = 2$ keV.
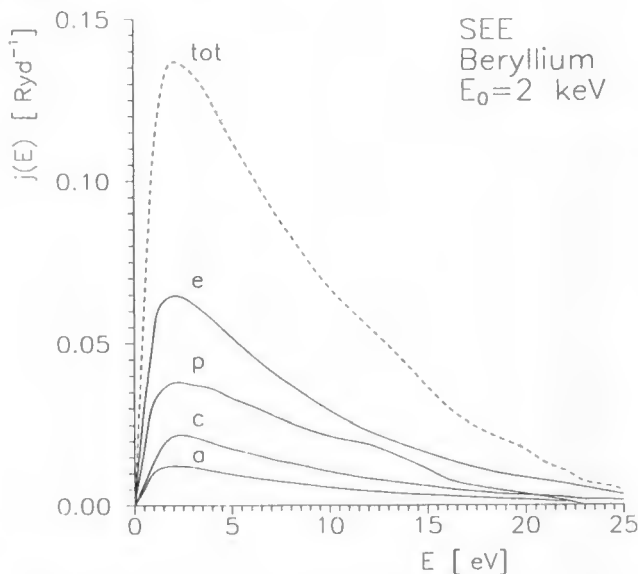

Figure 11. Energy distribution of SE for Be. Contributions from different excitation mechanisms: excitation of single conduction electrons (e), by decay of plasmons (p), of core electrons (c), and by Auger processes (a); tot = total. $E_0 = 2$ keV.

In the case of Al (Fig. 9a), we obtain almost agreement between theory and experiment. In the case of Mg (Fig. 9b), the calculated values for the electron yield are distinctly below the experimental data. In the case of Be (Fig. 9c), the situation is reversed. Up to now, there is no simple explanation of the discrepancies between theory and experiment for Mg and Be. Some comments related to possible improvements of the theory are discussed below in **Discussion and Conclusions**.

Results for the Energy Spectra of SE at Low Energies

Compared with the ion-induced KEE there is, in the case of SEE, only a restricted number of experimental results for the energy distribution of emerging electrons. As mentioned in **Excitation Processes**, the SE spectra show, in the case of Mg, the so-called plasmon shoulder (Jenkins and Chung, 1972). Using the values for the model potential Fourier coefficients $V_{\vec{K}}$ given in Table 1, our calculation leads for Mg to the spectra of SE shown in Figure 10 for $E_0 = 2$ keV. The shape of the spectra will be nearly the same at higher primary energies. Besides the cascade maximum at ≈ 2 eV, a second strongly pronounced peak appears around 7 eV which is attributed to the excitation of conduction electrons by plasmon decay. Especially, the plasmon decay by interband processes related to the reciprocal lattice vector $\vec{K}_4$ {which is essential only in a restricted energy range (see

Fig. 3)} is responsible for the additional peak in the energy distribution of emerging electrons. In the measured energy spectra of SE no such additional peak can be seen. In **Discussion and Conclusions**, some reasons will be discussed which lead to a reduction of the contribution of excitation of conduction electrons by plasmon decay to the number of emitted electrons.

Independent from the relative importance of the $\vec{K}_4$-contribution to S_p, our calculations lead in every case to a plasmon shoulder in the energy spectra of SE at $\hbar\omega_p - \Phi \approx 7.2$ eV which agrees very well with the energetic position given in the experiment.

In the case of Be, no plasmon shoulder can be seen in the spectrum of emerging electrons measured by Koshikawa *et al.* (1974). Whereas for Al and Mg, the relatively small plasmon damping ($\Gamma_0 = 0.5$ eV for Al and $\Gamma_0 = 0.7$ eV for Mg, see Table 1) leads to a distinct decrease of the excitation rate by plasmon decay at energies beyond $\hbar\omega_p(0) + E_F$. We obtain, in the calculations for Be, a moderate decrease of the excitation rate (see Figs. 3b and 4b) by reason of the large plasmon damping (≈ 2-4 eV, see Table 1). In this way, the plasmon shoulder which appears in the spectra of emerging electrons of Al and Mg will be suppressed to a large extent in Be as shown in Figure 11 (using $\Gamma_0 = 4$ eV in the calculations) in accordance with the experiment. Unfortunately, by reason of the restricted number of experimental results for the energy spectra of emitted electrons, our comparison between experimental and calcu-
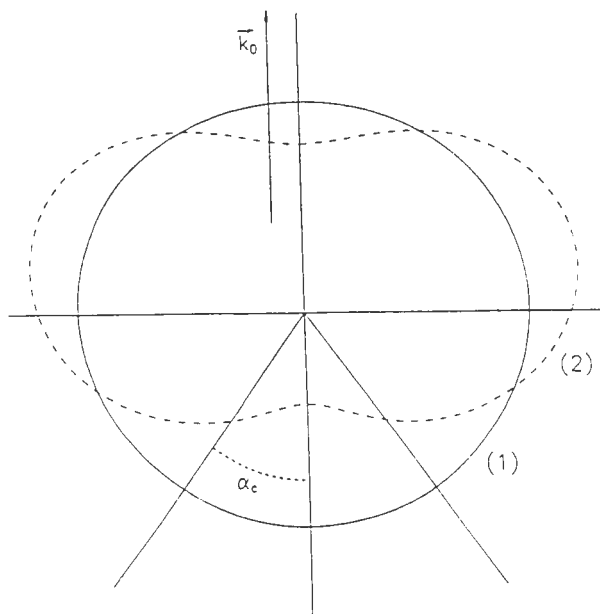
Figure 12. Angular distribution of the density $N(E,\vec{u})$ of inner excited electrons in the case of excitation of single conduction electrons including (1) and neglecting (2) elastic scattering. The excitation energy is measured from the vacuum level, $\vec{K}_0$ denotes the wave vector of the PE, and α_c is the aperture of the escape cone.

----

lated spectra allows no final statements about the role of the excitation by plasmon decay, especially for Be.

The Role of Different Scattering Processes

Inelastic scattering processes, especially the electron-electron scattering, are responsible for the accumulation of excited electrons at low energies and therefore, for the well-known cascade maximum in the energy spectra of emerging SE. Besides the electron-electron contributions, the transition function $W_1^{\sigma(inel)}$ contains contributions which describe the transition of the excited electron from the state $\vec{K}'(E',\vec{u}')$ with $E' > (1+q_c/k_F)^2 E_F$ to the state $\vec{K}(E,\vec{u})$ by excitation of a plasmon as well as the delayed process of the excitation of a conduction electron into the state $\vec{K}$ by the subsequent decay of these plasmons. This latter process of generating SE by decay of plasmons which are excited by energetic electrons (obtained by different excitation processes: S_e, S_c, S_a), leads to a more pronounced plasmon shoulder in the energy distribution of emerging electrons. With respect to the electron yield we obtain an enhancement of δ_0 if we take into account the transition processes related to plasmon decay. The enhancement is nearly constant in the whole range of primary energies (1 to 20 keV): $\approx 2\%$ for Al, 15% for Mg, and 14% for Be.
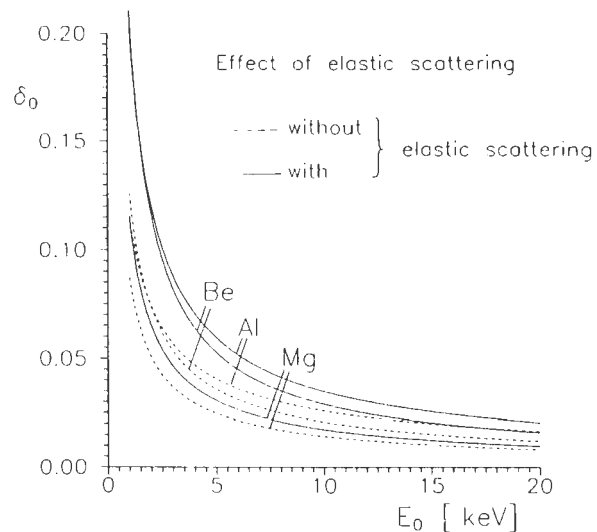

Figure 13. Primary energy dependence of the electron yield δ_0 for Al, Mg, and Be. Effect of elastic scattering: solid lines (with elastic scattering), dashed lines (without elastic scattering).

It should be noted that by reason of the marked anisotropy of the different excitation rates, it is of fundamental importance to include the elastic scattering in the description of the SEE. In particular, it is the excitation of single conduction electrons which is strongly anisotrop as shown for Be in Figure 2. Besides the inelastic electron-electron scattering, the elastic scattering of excited electrons is mainly responsible for the nearly isotropic angular distribution of internal electrons. This will be demonstrated for Be in Figure 12 for the case of excitation of single conduction electrons. The current density of emerging electrons $j(E,\vec{u})$ is determined by that part of the internal distribution $N(E',\vec{u}')$ which is restricted to the escape cone. Within this angular region, we obtain a large enhancement of the number of inner excited electrons by reason of elastic scattering. The enhancement effect of elastic scattering on the electron yield δ_0 for all three metals, including all excitation mechanisms, is shown in Figure 13. For Be, elastic scattering leads to the largest enhancement of the yield compared with the other metals because the strongly anisotropic excitation of single conduction electrons is the most important excitation mechanism in this metal (see Fig. 8c).

Discussion and Conclusions

In order to obtain more general statements about the role of different excitation and scattering mechanisms with respect to SEE from solids, especially metals, calculations were performed for different simple metals. It
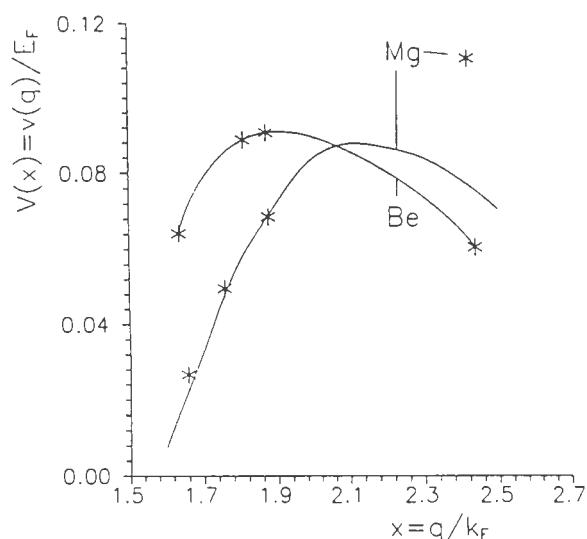
Figure 14. Fourier transform of the model potential for Mg and Be in the wave number region of relevant reciprocal lattice vectors $\vec{K}_i$ ($i \le 4$). Mg: model potential Fourier coefficients given by Cohen and Heine (1970) (marked by stars) and model potential of Heine and Abarenkov (Animalu and Heine, 1965) (solid line). Be: Ashcroft model potential (Ashcroft, 1968) (solid line). The stars mark the Fourier coefficients at the reciprocal lattice vectors.

---

is remarkable that the results obtained up to now for Al cannot be generalized to other simple metals without explicit calculations.

Starting from the microscopic description of SEE based on a transport equation formalism discussed in **Basic Considerations Concerning the Description of SEE Within the Transport Equation Formalism and Excitation Processes**, calculations of the emission characteristics were performed for Mg and Be. Besides the differences in the electronic structure of these metals (density of conduction electrons, type and energetic position of the core levels, see Table 1), the special features related to the plasmon, especially the plasmon damping, are responsible for the different role of several excitation processes in these metals compared with Al. The description of interband processes which govern, besides the plasmon damping, also the excitation of conduction electrons by plasmon decay within a model potential formalism, requires the knowledge of the Fourier transform of this model potential at the different reciprocal lattice vectors (denoting the different interband processes within the extended zone scheme). In the case of Mg, agreement between calculated (Sturm, 1976) and measured (Kloos, 1973) plasmon damping can be achieved using the model potential Fourier coefficients given by Cohen and Heine (1970). On the other hand, using this model

potential, we obtain the double peak structure in the energy distribution of emitted electrons shown in Figure 10 in contradiction to the experimental results. The height of the peak around 7 eV will be determined essentially by the magnitude of the model potential Fourier coefficient related to $\vec{K}_4$. It is well-known that an adequate description of all electronic properties of simple metals using one and the same model potential is impossible. Therefore, other model potentials were used in the past with varying degrees of success. A widely used model potential is given by Animalu and Heine (1965). In Figure 14, we compare this model potential with the model potential used in our calculations for Mg. With respect to the interband processes related to the reciprocal lattice vectors $\vec{K}_i$ ($i = 1,2,3$) with $|\vec{K}_i| < 2k_F$ the $V_{\vec{K}}$ are determined by the Fermi surface geometry. Therefore, for both model potentials we have nearly the same numerical values for the corresponding Fourier coefficients. However, for the model potential of Animalu and Heine (1965) the Fourier coefficient $V_{\vec{K}}$ is distinctly smaller than the corresponding value for the Ashcroft potential. This leads to a considerable reduction of the peak height at ≈ 7 eV compared with the cascade maximum at ≈ 2 eV (see Fig. 10) and therefore, to a better agreement between theory and experiment. On the other hand, using the model potential of Animalu and Heine in the evaluation of the plasmon damping according to Sturm (1976), agreement between theoretical and experimental results disappears.

Another point should be noted which leads to a better agreement between theory and experiment with respect to the energy distribution of emerging electrons as well as with respect to the electron yield. It was mentioned at the end of **Basic Considerations Concerning the Description of SEE Within the Transport Equation Formalism** that we obtain a reduction of the elastic mfp compared with the inelastic one at low energies by using the phase shift data obtained by Heinz (personal communication, 1995). This reduction of l^{el} leads to an enhancement of the contribution resulting from the strongly anisotropic excitation of single conduction electrons and, therefore, to an enhancement of the cascade peak compared to the peak related to plasmon decay.

A short comment concerning the widely used free-electron-gas model for the description of the electronic structure of simple metals will be given. In RPA, the elementary excitations within this model are the plasmon and the electron-hole-pair excitations. The undamped plasmon is restricted to wave numbers below the cut-off wave number q_c. In real metals, plasmon damping takes place. In order to describe this plasmon damping, it is necessary to go beyond the free-electron-gas picture. Interband processes which govern the plasmon damping

are also responsible for the generation of SE. In order to determine this generation of SE by decay of plasmons, the electronic structure can be described by perturbation theory with respect to a suitable chosen model potential. However, there are other deviations from the simple free-electron-gas picture which should be taken into account in a final version of the theory. By measurements of the inelastic X-ray scattering, it has been shown that the elementary excitation spectrum in the region of the electron-hole-pair continuum is more complicated than predicted by the free-electron-gas model in RPA. For Al and Be, a double peak behavior of the electronic structure factor $S(q,\omega) \sim Im[1/\epsilon(q,\omega)]$ was obtained for wave numbers beyond q_c (Vradis and Priftis, 1985; Schülke *et al.*, 1989, 1993). Therefore, in the corresponding spectrum of elementary excitations we obtain, for instance for Be, a lower branch which is plasmon-like and an upper branch which shows considerable dispersion. For large wave numbers q, this latter branch tends to become parallel to $\hbar^2 q^2 / 2m$. According to Maddocks *et al.* (1994a,b) and Fleszar *et al.* (1995), the double peak behavior of $S(q,\omega)$ can be described by taking into account the lattice structure of these metals. Up to now there is no straightforward way to include these modifications of the elementary excitation spectrum in a description of the excitation of conduction electrons.

Finally, we can state that with respect to the formation of the SE signal in the STEM, no general statement can be given. What kind of excitation mechanism is the dominant one in creating SE depends on the specific electronic properties of the solid (metal). Further explicit calculations for other materials up to high primary energies are needed in order to obtain conclusive results concerning the origin of the SE signal. On the other hand, it would be desirable to extend the coincidence experiments mentioned in the introduction to that type of solids which allow direct comparison with theoretical predictions concerning the basic processes of SE generation.

Acknowledgement

References

Akkerman A, Gibrekhterman A, Breskin A, Chechik R (1992) Monte Carlo simulations of secondary electron emission from CsI, induced by 1-10 keV X-rays and electrons. J. Appl. Phys. **72**, 5429-5436.

Akkerman A, Breskin A, Chechik R, Gibrekhterman A (1993) Secondary electron emission from alkali halides induced by X-rays and electrons. In: Ionization of Solids by Heavy Particles. Baragiola RA (ed.). Plenum Press, New York. pp. 359-380.

Animalu AOE, Heine V (1965) The screened model potential for 25 elements. Phil. Mag. **12**, 1249-1270.

Ashcroft NW (1968) Electron-ion pseudopotential in the alkali metals. J. Phys. **C1**, 232.

Bachlechner M (1994) Two-Pair effects. In: Simple Metals and Semiconductor Structures. PhD Thesis, University of Linz, Austria.

Bennet AJ, Roth LM (1972) Effect of primary electron diffusion on secondary electron emission. Phys. Rev. **B5**, 4309-4324.

Bindi R, Lanteri H, Rostaing P (1980a) A new approach and resolution method of the Boltzmann equation applied to secondary electron emission by reflection from polycrystalline aluminum. J. Phys. D: Appl. Phys. **13**, 267-280.

Bindi R, Lanteri H, Rostaing P (1980b) Application of the Boltzmann equation to secondary electron emission from copper and gold. J. Phys. D: Appl. Phys. **13**, 461-470.

Bindi R, Lanteri H, Rostaing P (1987) Secondary electron emission induced by electron bombardment of polycrystalline metallic targets. Scanning Microsc. **1**, 1475-1490.

Bindi R, Lanteri H, Rostaing P (1988) Transport model of scattering processes of keV electrons in aluminum. Surf. Sci. **197**, 295-316.

Bleloch AL (1989) Secondary electron spectroscopy in a dedicated scanning transmission electron microscopy. Ultramicroscopy **29**, 147-152.

Bleloch AL, Howie A, Milne RH (1989) High resolution secondary electron imaging and spectroscopy. Ultramicroscopy **31**, 99-110.

Brauer W (1972) Einführung in die Elektronentheorie der Metalle (Introduction to the Electron Theory of Metals). Akademische Verlagsgesellsch. Geest und Portig, Leipzig, Germany. pp. 236-244.

Bronshtein IM, Fraiman BS (1969) Secondary Electron Emission. Nauka, Moscow, Russia. pp. 200-212. (in Russian)

Cailler M, Ganachaud JP (1990a) Secondary electron emission from solids. I. Secondary electron spectroscopy. Scanning Microsc. Suppl. **4**, 57-79.

Cailler M, Ganachaud JP (1990b) Secondary electron emission from solids. II. Theoretical descriptions. Scanning Microsc. Suppl. **4**, 81-110.

Cheng SC (1987) Localization distance of plasmons excited by high-energy electrons. Ultramicroscopy. **21**, 291-292.

Chung MS, Everhart TE (1977) Role of plasmon decay in secondary electron emission in nearly-free-electron metals. Application to aluminum. Phys. Rev. **B15**,

4699-4715.

Cohen ML, Heine V (1970) The fitting of pseudo-potentials to experimental data and their subsequent applications. In: Solid State Physics. Vol. 24. Academic Press, New York. pp. 38-248.

Devooght J, Dubus A, Dehaes JC (1987) Improved age-diffusion model for low-energy electron transport in solids. I. Theory. Phys. Rev. **B36**, 5093-5109.

Devooght J, Dehaes JC, Dubus A, Cailler M, Ganachaud JP (1991) Theoretical description of secondary electron emission induced by electron or ion beams impinging on solids. In: Particle Induced Electron Emission I. In: Springer Tracts in Modern Physics. Vol. 122. Springer, New York. pp. 67-128.

Devooght J, Dubus A, Dehaes JC (1992) Approximate solution of the Boltzmann electron transport equation in a semi-infinite medium and surface correction to the secondary electron yield. Nucl. Instrum. Meth. **B67**, 650-654.

Ding ZJ, Shimizu R (1988) Monte Carlo study of backscattering and secondary electron generation. Surf. Sci. **197**, 539-554.

Dubus A, Devooght J, Dehaes JC (1987) Improved age-diffusion model for low-energy electron transport in solids. II. Application to secondary emission from aluminum. Phys. Rev. **B36**, 5110-5119.

Dubus A, Devooght J, Dehaes JC (1990) Approximate solutions of the Boltzmann equation for secondary electron emission: Results and comparison to experiments. Scanning Microsc. **4**, 1-20.

Dubus A, Dehaes JC, Ganachaud JP, Hafni A, Cailler M (1993) Monte Carlo evaluation of the influence of the interaction cross-sections on the secondary electron emission yields from polycrystalline aluminum targets. Phys. Rev. **B47**, 11056-11073.

Eisenberger P, Platzman PM, Pandey KC (1973) Investigation of X-ray plasmon scattering in single-crystal Beryllium. Phys. Rev. Lett. **31**, 311-314.

Fleszar A, Quong AA, Eguiluz AG (1995) Band-structure and many-body effects in the dynamical response of aluminum metal. Phys. Rev. Lett. **74**, 590-593.

Ganachaud JP, Cailler M (1979a) A Monte Carlo calculation of the secondary electron emission of normal metals. I. The model. Sur. Sci. **83**, 498-518.

Ganachaud JP, Cailler M (1979b) A Monte Carlo calculation of the secondary electron emission of normal metals. II. Results for aluminum. Surf. Sci. **83**, 519-530.

Gryzinski M (1965a) Two particle collisions. I. General relations for collisions in the laboratory system. Phys. Rev. **138**, 305-321.

Gryzinski M (1965b) Two particle collisions. II. Coulomb collision in the laboratory system of coordinates. Phys. Rev. **138**, 322-335.

Gryzinski M (1965c) Classical theory of atomic collisions. I. Theory of inelastic collisions. Phys. Rev. **138**, 336-358.

Herman F, Skillman S (1963) Atomic Structure Calculations. Prentice Hall, Englewood Cliffs, NJ. pp. 6/1-6/23.

Hippler S (1988) Spezielle Aspekte der ioneninduzierten Elektronenemission aus Festkörperoberflächen: Eine Untersuchung von Strukturen im niederenergetischen Emissionsspektrum und zur Z_2-Abhängigkeit des Sekundärelektronen-emissionskoeffizienten (Special aspects of the ion-induced electron emission from surfaces: Investigation of structures in the emission spectra at low energies and of the Z_2-dependence of the electron yield). PhD Thesis, University of Giessen, Germany.

Jenkins LH, Jenkins MF (1972) The auger satellite and other characteristic events in Mg secondary electron spectra. Surf. Sci. **33**, 159-171.

Kaneko T (1990) Energy distribution of secondary electrons emitted from solid surfaces under electron bombardment. I. Theory. Surf. Sci. **237**, 327-336.

Kawata J, Ohya K (1994) Surface roughness effect on secondary electron emission from Beryllium under electron bombardment. J. Phys. Soc. Japan **63**, 795-806.

Kloos T (1973) Plasmaschwingungen in Al, Mg, Li, Na und K angeregt durch schnelle Elektronen (Plasma oscillations in Al, Mg, Li, Na, and K excited by fast electrons). Z. Physik **265**, 225-238.

Koshikawa T, Shimizu R (1974) A Monte Carlo calculation of low-energy secondary electron emission from metals. J. Phys. D: Appl. Phys. **7**, 1303-1317.

Koshikawa T, Goto K, Shimizu R, Ishikawa K (1974) Secondary electron spectra from a Be layer evaporated on Cu. J. Phys. D: Appl. Phys. **7**, L174-L177.

Kotera M, Kishida T and Suga H (1990) Monte Carlo Simulation of secondary electrons in solids and its application for scanning electron microscopy. Scanning Microsc. Suppl. **4**, 111-126.

Krane KJ (1978) Dispersion and damping of volume plasmons in polycrystalline aluminum and indium. J. Phys. F: Metal Physics **8**, 2133-2137.

Krishan V, Ritchie RH (1970) Anomalous damping of volume plasmons in polycrystalline metals. Phys. Rev. Lett. **24**, 1117-1119.

Luo S, Joy DC (1990) Monte Carlo calculation of secondary electron emission. Scanning Microsc. Suppl. **4**, 127-146.

Maddocks NE, Godby RW, Needs RJ (1994a) *Ab initio* calculations of the dynamic response of beryllium. Phys. Rev. **B49**, 8502-8505.

Maddocks NE, Godby RW, Needs RJ (1994b) Band structure effects in the dynamic response of aluminum. Europhys. Lett. **27**, 681-686.

Manson ST (1972) Inelastic collisions of fast charged particles with atoms: Ionization of the aluminum L shell. Phys. Rev. A **6**, 1013-1024.

Müllejans H, Bleloch AL, Howie A, McMullan D (1991) Coincidence between secondary and energy loss electrons in STEM. Beitr. Elektronenmikroskop. Direktabb. Oberfl. **24**, 93-98.

Müllejans H (1992) Secondary electron emission in coincidence with primary energy losses. PhD Thesis, University of Cambridge, U.K.

Ohya K (1994) Secondary electron emission and backscattering from a metal surface under low-energy positron and electron bombardment. Jap. J. Appl. Phys. **33**, 4735-4736.

Paasch G (1969) Influence of interband transitions on plasmons in the alkali metals: Pseudopotential calculation. Phys. Stat. Sol. **38**, K123-K126.

Pendry JB (1974) Low Energy Electron Diffraction. Academic Press, London, U.K. Appendix 4. pp. 345-367.

Pijper FJ, Kruit P (1991) Detection of energy-selected secondary electrons in coincidence with energy-loss events in thin carbon foils. Phys. Rev. **B44**, 9192-9200.

Puff H (1962) Zur Theorie der Sekundärelektronen-emission von Metallen am Modell freier Elektronen (On the theory of secondary electron emission of metals within the free electron model). Phys. Stat. Sol. **2**, 1699-1712.

Puff H (1964) Zur Theorie der Sekundärelektronen-emission. Der Transportprozeß. I. Formulierung des Problems (On the theory of secondary electron emission. The transport process. I. Formulation of the problem). Phys. Stat. Sol. **4**, 125-138.

Quinn JJ (1962) Range of excited electrons in metals. Phys. Rev. **126**, 1453-1457.

Ritchie RH (1981) Quantal aspects of the spatial resolution of energy loss measurements in electron microscopy. Phil. Mag. **A44**, 931-942.

Ritchie RH, Howie A, Echenique PM, Basbas GJ, Ferrell TL, Ashley JC (1990) Plasmons in scanning transmission electron microscopy electron spectra. Scanning Microsc. Suppl. **4**, 45-56.

Ritchie RH, Hamm RN, Ashley JC, Echenique PM (1991) Electron spectra in solids. In: Interaction of Charged Particles with Solids and Surfaces. Gras-Marti A, Urbassek HM, Arista NR, Flores F (eds.). Plenum Press, New York. pp. 197-225.

Rösler M (1991) Contribution of Auger processes to the particle-induced electron emission from nearly-free-electron metals. Nucl. Instrum. Meth. **B58**, 309-312.

Rösler M (1993) Ion-induced kinetic electron emission of metals: Comparative studies of excitation and scattering mechanisms. Nucl. Instrum. Meth. B **78**, 263-267.

Rösler M (1994a) Plasmon effects in the particle-induced kinetic electron emission from solids. Scanning Microsc. **8**, 3-22.

Rösler M (1994b) Plasmon effects in the particle-induced kinetic electron emission from nearly-free-electron metals. Nucl. Instrum. Meth. **B90**, 537-541.

Rösler M (1995) Theory of particle-induced kinetic electron emission from simple metals: Comparative studies of different excitation and scattering mechanisms for Al, Mg, and Be. Appl. Phys. **A61**, 595-607.

Rösler M, Brauer W (1981a) Theory of secondary electron emission. I. General theory for nearly-free-electron metals. Phys. Stat. Sol. (b) **104**, 161-175.

Rösler M, Brauer W (1981b) Theory of secondary electron emission. II. Application to aluminum. Phys. Stat. Sol. (b) **104**, 575-587.

Rösler M, Brauer W (1988) Theory of electron emission from solids by proton and electron bombardment. Phys. Stat. Sol. (b) **148**, 213-226.

Rösler M, Brauer W (1991) Theory of electron emission from nearly-free-electron metals by proton and electron bombardment. In: Particle Induced Electron Emission I; Springer Tracts in Modern Physics. Vol. 122. Springer, New York. pp. 1-65.

Rösler M, Brauer W (1992) Contribution of core states to the emission properties in the particle-induced electron emission of metals. Nucl. Instrum. Meth. **B67**, 641-645.

Scheinfein M, Muray A, Isaacson M (1985) Electron energy loss spectroscopy across a metal insulator interface at sub-nanometer spatial resolution. Ultramicroscopy **16**, 233-240.

Scheinfein MR, Drucker J, Weiss JK (1993) Secondary-electron production pathways determined by coincidence electron spectroscopy. Phys. Rev. **B47**, 4068-4071.

Schou J (1980) Transport theory for kinetic emission of secondary electrons from solids. Phys. Rev. **B22**, 2141-2174.

Schou J (1988) Secondary electron emission from solids by electron and proton bombardment. Scanning Microsc. **2**, 607-632.

Schülke W, Nagasawa H, Mourikis S, Kaprolat A (1989) Dynamic structure of electrons in Be metal by inelastic x-ray scattering spectroscopy. Phys. Rev. **B40**, 12215-12228.

Schülke W, Schulte-Schrepping H, Schmitz JR (1993) Dynamic structure of electrons in Al metal studied by inelastic x-ray scattering. Phys. Rev. **B47**, 12426-12436.

Seiler H (1967) Einige aktuelle Probleme der Sekundärelektronenemission (Some problems of secondary electron emission). Z. angew. Physik **22**, 249-263.

Seiler H (1983) Secondary electron emission in the scanning electron microscope. J. Appl. Phys. **54**, R1-R18.

Seiler H (1984) Secondary electron emission. In: Electron Beam Interaction with Solids for Microscopy, Microanalysis and Microlithography. Kyser DF, Niedrig H, Newbury D, Shimizu R (eds). Scanning Electron Microscopy, Inc., AMF O'Hare, IL. pp. 33-42.

Shimizu R, Kataoka Y, Ikuta T, Koshikawa T, Hashimoto H (1976) A Monte Carlo approach to the direct simulation of electron penetration in solids. J. Phys. D: Appl. Phys. **9**, 101-114.

Shimizu R, Ding ZJ (1992) Monte Carlo modelling of electron-solid interaction. Rep. Progr. Phys. **55**, 487-531.

Smrčka L (1970) Energy band structure of aluminum by the augmented plane wave method. Czech. J. Phys. **B20**, 291-300.

Staub PF (1994) Bulk target backscattering coefficient and energy distribution of 0.5-100 keV electrons: An empirical and synthetic study. J. Phys. D: Appl. Phys. **27**, 1533-1537.

Streitwolf HW (1959) Zur Theorie der Sekundärelektronenemission von Metallen. Der Anregungsprozeß (On the theory of secondary electron emission from metals. The excitation process). Ann. Phys. **3**, 183-196.

Sturm K (1976) Pseudopotential theory of the width of the long wavelength plasmon in simple metals. Z. Pkysik **B25**, 247-253.

Sturm K (1977) Pseudopotential theory of the k-dependent plasmon line width in simple metals. Z. Physik **B28**, 1-7.

Sturm K (1982) Electron energy loss in simple metals and semiconductors. Adv. Phys. **31**, 1-64.

Tung CJ, Ritchie RH (1977) Electron slowing-down spectra in aluminum metal. Phys. Rev. **B16**, 4302-4313.

Vradis A, Priftis GD (1985) Dynamic structure factor $S(k,\omega)$ of beryllium by x-ray inelastic scattering experiments. Phys. Rev. **B 32**, 3556-3561.

Discussion with Reviewers

T. Kaneko: Though the possible physical processes in the source excitation were taken into account, a quantitative agreement between calculated and experimental results in the SE yield δ_0 from Mg and Be is not so good in comparison with that from Al. Namely, in the Mg case, the theory underestimates, and in the Be case, it overestimates. Of course, more data are necessary both in δ_0 and $j(E)$. A first idea to attack theoretically is to include the band structure. Does the author think that the way left is to take into account the band structure?
Author: We believe that with respect to the electron-electron scattering processes {excitation function S_e, contribution to the transition function $W^{\sigma(inel)}$}, band structure effects are of minor importance. On the other hand, in the description of processes which are related to the decay of plasmons via interband processes {excitation function S_p, contribution to the transition function $W^{\sigma(inel)}$}, the band structure is of fundamental importance. In order to avoid an unacceptably large numerical effort in the description of these processes, we have used a simple model potential approach.

Using the model potential coefficients given in the table (see appendix), the calculated plasmon damping rate $\Gamma(q)$ is distinctly below the experimental values. Other damping mechanisms discussed in the literature are not responsible for this discrepancy. An evaluation of the plasmon damping rate determined by interband processes, which takes into account the real band structure of the metals considered here, leads probably to a better agreement between theory and experiment. The same should be true with respect to the emission properties because plasmon damping and the excitation of electrons by plasmon decay are governed by the same type of interband processes.

T. Kaneko: The author mentions that the ISD escape condition overestimates the number of excited electrons by nearly 25%. Could inclusion of the boundary conditions lessen this discrepancy?
Author: Within the ISD model, we have used the simple classical description of the escape process based on the assumption of a sharp surface potential barrier and free electrons inside the target. Taking into account the boundary conditions related to this specular reflection model in the solution of the Boltzmann equation, the number of emerging electrons is reduced as mentioned above. This was shown in a model calculation by Devooght *et al.* (1992) using simple approximations for the different excitation and scattering quantities. Improvements with respect to the escape conditions are conceivable (quantum mechanical description of the transmission (Kaneko, 1990), realistic model of the surface barrier). In every case, the solution of the Boltzmann equation, taking into account the corresponding boundary conditions as well as the more elaborate expressions for the excitation and transition functions considered in the present paper, is beyond the scope of this work. Compared with the classical description of the escape process and the transport of excited electrons within the ISD model, the mentioned improvements of the theoretical description leads to a reduction of the number of emitted electrons. In this way, better agreement between theory and experiment can be obtained for Be. The opposite is the case for Mg.

J.P. Ganachaud: The relative importance of the differ-

ent excitation processes is not the same at low energies and at high energies. In your calculations, you do not account for the contribution of the backscattered electrons to the secondary yield δ. Do you expect that their introduction in your model could modify your conclusion significantly?

A. Dubus: You only calculate the incident primary part of the yield for δ_0. If you take into account the transport (and backscattering) of primary electrons, will your results about the importance of the excitation processes be changed?

Author: In contrast to the Monte Carlo treatment of the SEE, the inclusion of backscattered electrons in our model is not possible in a simple way. A first attempt with respect to a general treatment of the SEE based on the Boltzmann transport equation formalism which is valid also at low primary energies, including the effect of energy loss and deflection of the PE, was given by Bennet and Roth (1972) and Bindi et al. (1980a). According to these authors, the total excitation function including the backscattered electrons, is determined by the distribution function of PE (determined by a separate equation), as well as by the different excitation rates up to very low primary energies. However, at low primary energies (in the 100 eV range), the excitation of single conduction electrons as well as the excitation by plasmon decay (above the plasmon threshold), are the dominant excitation mechanisms. Therefore, if we take into account the backscattered electrons, the statement with respect to the relative importance of the different excitation processes in the keV range will possibly be changed. In contrast to the more elaborate treatment proposed by Bennet and Roth (1972) and Bindi et al. (1980a), a simple model calculation can be performed (Puff, 1962) in order to decide this question. Puff (1962) starts with the basic assumption that the states of the backscattered electrons are distributed with equal probability in the possible energy and angular intervals. Then, in the total excitation rate (expansion coefficient with respect to Legendre polynomials),

$$S_l^{tot}(E_0;E') = S_l(E_0;E') + \eta S_l^{bs}(E_0;E')$$

the excitation rate S^{bs} which belongs to the backscattered electrons is a simple functional of the excitation rate S determined by PE for primary energies below E_0.

J.P. Ganachaud: The secondary electrons, which take part in the cascade are responsible for a large part of the plasmon excitations. In this low energy domain, the dispersion of the bulk plasmon mode could have some importance. Do you think that the structures caused by the various interband processes which contribute to the bulk plasmon decay could be attenuated by introducing

this dispersion?

Author: In our calculations, we have used for the transition function, which describes the generation of plasmons by excited electrons and their subsequent decay by excitation of conduction electrons via interband processes, an approximate expression using the zero wave number limit for the different quantities which govern this transition function {see discussion of Eq. (6.11) in Rösler and Brauer (1991)}. In this way, the plasmon shoulder which is primarily determined by the excitation function S_p at the energetic position $\hbar\omega_p(0)-\Phi$ is enhanced. An improved calculation of the transition function taking into account the plasmon dispersion was performed for Al. In contrast to the approximate treatment mentioned before, there is now a small weakening of the plasmon shoulder. However, no significant changes take place with respect to the total electron yield.

J.P. Ganachaud: A correct determination of the model potential and of the importance of its various Fourier coefficients is apparently determining to predict the shape of the true secondary peak. Could it be possible to obtain additional information about the validity of the potential from the plasmon loss peak profile measured by electron energy loss spectroscopy?

Author: The excitation function S_p and the interband contribution of the plasmon damping rate $\Gamma(q)$ are governed by the same type of electronic transition processes. From the measurement of the plasmon line width by electron energy loss spectroscopy, we obtain values for the total plasmon damping rate. Besides the plasmon decay via interband processes, there are other decay processes discussed by Sturm (1982). Moreover, the interband contribution to the damping rate is given by a sum over all relevant interband processes which are related within the model potential formalism to the different Fourier coefficients of the model potential. Therefore, from the global information given by the measurements of the plasmon loss peak profile, no conclusive statement can be obtained about the validity of a chosen model potential.

R. Bindi: How do you explain the change in the relative predominant order between the different excitation functions (Figs. 7a,b) and their contribution to the electron yield δ_0 (Figs. 8a,b) and also between δ_0 in Figure 8b and the energy distribution (Fig. 10)?

Author: In order to obtain a definite statement about the contributions of the different excitation mechanisms to the electron yield, it is not sufficient to start from Figure 7. The reason is twofold: first, the energy dependent excitation functions shown in this figure correspond to the $l = 0$ component of the expansion of the excitation functions with respect to Legendre polynomi-

als. In a complete calculation of the emission properties, the anisotropy of the excitation rates (which is varying for the different excitation mechanisms) should be taken into account. Secondly, electrons with high excitation energies are more effective with respect to the generation of inner excited electrons at low energies via the transport process. In this way, for instance, especially in the case of the excitation of core electrons (S_c), the small number of excited electrons at high energies leads to a contribution to the electron yield which is comparable or larger than the contributions from the other excitation processes. With respect to the second part of the question, the answer is the following: in the calculation of the yield of true SE, the energy integration is extended up to 50 eV. In the case of excitation of core electrons, the number of emerging electrons in the energy range up to this value is considerably larger than the contribution from the excitation of single conduction electrons. In this way, we obtain for instance for $E_0 = 2$ keV $\delta_0^c > \delta_0^e$ (which apparently contradicts the conclusion which one obtains by inspection of Fig. 10).

R. Bindi: Do you think that the excitation of core electrons is overestimated in your model?
Author: In our model, the excitation of core electrons is given by the transition probability calculated with wave functions which take into account solid state properties (the core states are described by Bloch sums, the excited states are described by OPW's). Therefore, the conclusion is justified that we obtain in this way an improved description of the core excitation rate compared with Gryzinski's model, used up to now in all calculations of the contribution of core electrons to the emission properties published by other authors.

A. Dubus: You have extended your model developed for aluminum to other NFE metals: Mg and Be. What is your opinion about the extension of your model to other metals (Au, Cu, Ag,...), semiconductors, insulators,...?
Author: With respect to the processes related to inner shell excitations, the extension of our model to other solids is possible with minor modifications. However, with respect to the processes related to the excitation of conduction electrons in non-NFE metals or of valence band electrons in semiconductors, a simple extension of our model is impossible. The real electronic structure in these materials is responsible for the special features related to the interaction of the PE with the elementary excitations of the target electron system. Especially, the appearance of plasmons as a well defined elementary excitation is strongly related to the real electronic structure. The simple model potential description of plasmon effects in NFE metals cannot extended to other mater-

ials. Calculations of scattering properties related to the conduction electron system for non-NFE metals, or, for instance, carbon, using the free electron model with a corresponding electron density parameter r_s (neglecting plasmon effects) are only suitable to obtain qualitative statements with respect to the emission characteristics of these metals.

A. Dubus: You neglect surface plasmons in your model. However, even for perpendicular incidence, a structure can be seen in the energy spectrum of electrons emitted from Al for instance. If you incorporate surface plasmons, will your results about the importance of excitation processes be changed?
J. Schou: Surface plasmons are neglected in the text. How large is the contribution from these plasmons? It is known that surface plasmons are as important as bulk plasmons in the spectra of electron loss spectroscopy, and that they show comparable structures in the spectra of the secondaries.
Author: Surface plasmons can be incorporated in the theoretical description of the SEE as discussed by Chung and Everhart (1977) and Rösler (1994a). Explicit calculations were performed by Chung and Everhart (1977). It was shown by these authors that a structure in the energy spectra of emerging electrons appear which is related to the decay of surface plasmons. On the other hand, these calculations show that with respect to the electron yield this mechanism is of minor importance. Therefore, the statement about the relative importance of different excitation mechanisms given in the present paper does not change significantly if we take into account surface plasmons.

A. Dubus: Other authors have used "simplified" models for the electron interaction cross-sections {Ganachaud and Cailler's model for plasmon decay (Ganachaud and Cailler, 1979a); Gryzinski's formalism (Gryzinski, 1965a,b,c;...}. What is your opinion about these simplified models?
Author: The mentioned simplified models concerning especially the plasmon decay and the description of inner shell excitations by Gryzinski's formula are useful in order to obtain qualitative results for different materials. Using these models, the numerical effort for the calculation of the emission characteristics is drastically reduced compared with the more elaborate calculation presented here. In order to obtain quantitative results for different materials, a description of the excitation and scattering processes starting from first principles seems to be essential. An adequate description of the plasmon decay and the inner shell excitations must take into account the special features of the electronic structure of the solid.